



## Research article

## Investigation of verapamil-induced cardiorenal dysfunction and compensatory ion regulation in zebrafish embryos



Jiun-Lin Horng<sup>a,1</sup>, Bu-Yuan Hsiao<sup>b,c,d</sup>, Wen-Ting Lin<sup>e</sup>, Tzu-Ting Lin<sup>a</sup>, Ching-Yen Chang<sup>a</sup>, Li-Yih Lin<sup>f,\*</sup>

<sup>a</sup> Department of Anatomy and Cell Biology, School of Medicine, College of Medicine, Taipei Medical University, Taipei 11031, Taiwan

<sup>b</sup> Division of Cardiology and Cardiovascular Research Center, Department of Internal Medicine, Taipei Medical University Hospital, Taipei 11031, Taiwan

<sup>c</sup> Division of Cardiology, Department of Internal Medicine, School of Medicine, College of Medicine, Taipei Medical University, Taipei 11031, Taiwan

<sup>d</sup> Taipei Heart Institute, Taipei Medical University, Taipei 11031, Taiwan

<sup>e</sup> Affiliated Senior High School of National Taiwan Normal University, Taipei 10658, Taiwan

<sup>f</sup> Department of Life Science, National Taiwan Normal University, Taipei 11677, Taiwan

## ARTICLE INFO

Edited by Martin Grosell

## Keywords:

Cardiorenal failure

Development

Edema

Skin

Kidney

## ABSTRACT

The purpose of the present study was to investigate the development of verapamil-induced cardiorenal failure and the response of epidermal ionocytes in zebrafish embryos to this syndrome. Zebrafish embryos were exposed to verapamil for 24 h at different developmental stages (48, 72, and 96 h post-fertilization). The exposure resulted in the generation of edema in the pericardial and yolk sac regions, with more-pronounced effects observed in later-stage embryos. Cardiac parameters showed a suppressed heart rate at all stages, with a more-significant effect appearing in later stages. Verapamil also affected cardiac parameters including the end-diastolic volume (EDV), end-systolic volume (ESV), ejection fraction (EF), and cardiac output (CO), indicating negative overall effects on cardiac performance. mRNA levels of heart failure markers (*nppa* and *nppb* genes) were upregulated in verapamil-exposed embryos at all stages. Renal function was impaired as FITC-dextran excretion was suppressed. A whole-embryo ion content analysis revealed significant increases in sodium and calcium contents in verapamil-exposed embryos. The density of epidermal ionocytes increased, and the apical membrane of ionocytes was enlarged, indicating upregulation of ion uptake. In addition, mRNA levels of several ion transporter genes (*rhcg1*, *slc9a3*, *atp6v1a*, *atp2b1a*, *trpv6*, and *slc12a10.2*) were significantly upregulated in verapamil-exposed embryos. In summary, prolonged exposure to verapamil can induce cardiorenal failure which triggers compensatory upregulation of ionocytes in zebrafish embryos.

## 1. Introduction

Currently, 64.3 million people worldwide have heart failure. In developed countries, the prevalence of heart failure is generally estimated to be 1% to 2% of the adult population, and the prevalence will increase as the population ages (Groenewegen et al., 2020). Heart failure is primarily caused by coronary artery disease (e.g., a heart attack), but other causes include valvular heart disease, cardiomyopathies, arrhythmias, and alcohol or drugs that are toxic to the heart (Kemp and Conte, 2012). Heart failure can lead to congestion or fluid buildup in the lungs and other tissues, causing symptoms such as shortness of breath, dyspnea, and edema of the lower extremities (Kemp and Conte, 2012).

A high percentage of patients with heart failure develop cardiorenal syndrome, which is defined as acute/chronic kidney dysfunction due to acute/chronic heart dysfunction (Ronco et al., 2018). This syndrome occurs when dysfunction in the heart, often leading to reduced cardiac output, initiates a chain reaction that affects kidney perfusion and function. Inadequate blood flow to the kidneys leads to the retention of water and sodium, disrupting the body's fluid balance. This imbalance further stresses the heart and exacerbates its dysfunction, creating a cyclical pattern that ultimately leads to compromised heart and kidney health (Ronco et al., 2018).

In recent decades, organizations such as the International Federation for the Protection of Animals (IFAW) and the Organization for Economic

\* Corresponding author at: Department of Life Science, National Taiwan Normal University, 88 Ting-Chow Rd., Sec. 4, Taipei 11677, Taiwan.

E-mail address: [linly@ntnu.edu.tw](mailto:linly@ntnu.edu.tw) (L.-Y. Lin).

<sup>1</sup> B.-Y. Hsiao and J.-L. Horng contributed equally to this study.

Cooperation and Development (OECD) have promoted the regulation of animal experimentation with the goal of reducing the use of laboratory animals. Under EU Directive 2010/63/EU, zebrafish embryos (within 120 h of fertilization) are considered an alternative to traditional laboratory animals (Strähle et al., 2012). In addition to ethical considerations, zebrafish embryos have a key advantage over traditional laboratory animals, such as mice and rats, in that they can be used for large-scale drug testing (Ali et al., 2012; Zon and Peterson, 2005). Therefore, creating alternative models using zebrafish embryos can facilitate the exploration of cardiorenal syndrome and the evaluation of drug efficacy.

The zebrafish heart is similar to the human heart in structure, function, and molecular pathways involved in heart development and regulation (Genge et al., 2016). The heart of a zebrafish embryo develops rapidly and is fully functional at 48 h post-fertilization (hpf). Numerous studies have shown that drugs that are clinically toxic to the heart can also damage the heart of zebrafish embryos, suggesting that zebrafish embryos can be used as a model for testing cardiotoxic drugs (Kithcart and MacRae, 2017). The transparency of zebrafish embryos allows direct observation by microscopy and assessment of cardiac function using image analysis techniques (Yalcin et al., 2017).

Living in hypotonic freshwater environments, zebrafish and other freshwater fishes face the challenge of water influx into their bodies by osmosis, and their kidneys can excrete excess water while reabsorbing essential ions, similar to the diuretic function of human kidneys (Poureetezadi and Wingert, 2016). The zebrafish kidney in the embryonic stage consists of a pair of pronephric tubes (pronephros) that begin to develop at 24 hpf and achieve full function by 48 hpf (Drummond, 2005). In addition, zebrafish acquire ions from water primarily through a group of ionocytes located in their gills and skin. These ionocytes function similarly to tubular cells in the human kidney and possess conserved mechanisms for transporting ions such as  $\text{Na}^+$ ,  $\text{Cl}^-$ , and  $\text{Ca}^{2+}$  uptake and  $\text{H}^+$ ,  $\text{NH}_4^+$ , and  $\text{K}^+$  secretion (Hwang et al., 2011; Hwang and Lin, 2013). Zebrafish depend on the coordinated action of ionocytes and renal tubules to maintain osmotic, ionic, and pH balance.

Previous investigations utilized genetic manipulation to establish a zebrafish model of heart failure (Narumanchi et al., 2021). Recent research utilized verapamil to induce heart failure in zebrafish embryos and used the model for drug testing (Li et al., 2022; Zhu et al., 2018). Verapamil, a cardiac L-type calcium channel blocker, is clinically used to treat cardiac arrhythmias, hypertension, and angina (Hofer et al., 1993). However, those zebrafish studies exclusively focused on cardiac effects after 30 min of verapamil treatment at 48 hpf and did not examine renal effects, which may require longer verapamil treatment. The present study aimed to address these knowledge gaps and, in particular, to investigate how epidermal ionocytes respond to cardiorenal dysfunction. We hypothesized that prolonged verapamil treatment might lead to the development of cardiorenal failure, prompting compensatory ion regulation by ionocytes.

We treated zebrafish embryos at different developmental stages (48–72, 72–96, and 96–120 hpf) with verapamil and evaluated cardiac parameters (including the heart rate, ventricular volume, stroke volume, ejection fraction, and cardiac output), renal parameters (such as pericardial and yolk sac edema and FITC-dextran clearance), and genes indicative of heart failure (*nppa* and *nppb*) to investigate the progression of cardiorenal failure. In addition, ion contents (sodium, calcium, and potassium contents), ionocyte numbers and morphology, and ion transporter gene expressions (*rhcg1*, *slc9a3*, *atp6v1a*, *atp2b1a*, *trpv6*, and *slc12a10.2*) were examined to reveal how epidermal ionocytes respond to cardiorenal failure.

## 2. Materials and methods

### 2.1. Experimental animals

Zebrafish (*Danio rerio*; AB strain; 8–9 months of age) were obtained

from the Zebrafish Core Laboratory of Taipei Medical University. They were housed in a zebrafish culture system with water temperature maintained at 28 °C and a light/dark cycle of 14/10 h. Their diet consisted of fish pellets and brine shrimp fed twice daily. Levels of ammonia and nitrite in the tank water were assessed weekly using aquaculture kits (AZ24010; AZOO, Taipei, Taiwan), and the readings consistently remained below recommended thresholds. In the morning, five pairs of mature zebrafish were placed in a 2-L breeding tank for mating. Fertilized eggs were collected within 2 h after mating and then incubated in artificial freshwater (AFW) with essential ion concentrations similar to those found in local tap water (Horng et al., 2017; Lin et al., 2019). The Animal Care and Use Committee of National Taiwan Normal University reviewed and approved the use of adult zebrafish in this study. Zebrafish embryos used in this study were <120 h old and therefore did not require approval.

### 2.2. Verapamil preparation and administration

Verapamil powder (verapamil hydrochloride; cat. no.: HY-A0064; purity: 99.98 %; MedChemExpress; Monmouth Junction, NJ, USA) was dissolved in dimethyl sulfoxide (DMSO, Sigma-Aldrich; Burlington, MA, USA) to create a stock solution of 100 mM, which was then diluted with AFW to achieve final concentrations of 100 and 200  $\mu\text{M}$  (contains 0.1 and 0.2 % DMSO, respectively). Verapamil concentrations were determined based on preliminary tests to ensure that the embryo could survive exposure without significant mortality. A control solution containing 0  $\mu\text{M}$  verapamil (0.2 % DMSO only) in AFW was utilized for comparison. Verapamil treatment involved immersing embryos at three developmental stages (48–72, 72–96, and 96–120 hpf) in a verapamil solution for 24 h. Each well of a 24-well plate contained 1 mL of solution with 10 embryos. The specific number of embryos used in each experiment is detailed in subsequent sections. Embryos were incubated in plates at 28 °C with a light/dark cycle of 14 h light and 10 h dark using a growth incubator (PGC–600C, Jaan-Yuh Instrument, Taipei, Taiwan).

### 2.3. Measurement of pericardial and yolk sac edema

A morphometric analysis was used to assess the pericardial cavity and yolk sac areas as indicators of edema. After exposure to verapamil, 15 embryos from each group were randomly selected for analysis ( $n = 15$  from three experiments). Digital images of embryos were taken with a digital camera (A5000, Sony, Tokyo, Japan) attached to a stereomicroscope (Stemi 508, Zeiss, Oberkochen, Germany). The embryos were anesthetized with tricaine (100 mg/L; Sigma-Aldrich, St. Louis, MO, USA) before imaging. The pericardial cavity and yolk sac areas were quantified using NIH ImageJ software (<https://imagej.net/ij/index.html>).

### 2.4. Measurement of cardiovascular parameters

Zebrafish embryos were anesthetized with tricaine in a Petri dish, and the lateral view of heart images was video-recorded with a digital camera (Sony Alpha ILCE-A6300) mounted on an upright microscope (BX51WI, Olympus, Tokyo, Japan). The video resolution and frame rate were set to 3840  $\times$  2160 and 30 frames/s, respectively. The water temperature was maintained at 28 °C during video recording. For each experimental group, 15 embryos ( $n = 15$  collected from three experiments) were randomly selected for measurement of cardiac parameters following the protocol described in a previous study (Hsiao et al., 2024). In brief, video clips were recorded and then reviewed frame by frame using Tracker software (<https://physlets.org/tracker/>). At the end-diastole (ED) and end-systole (ES) stages of the heart, images of the ventricle were captured from video clips and further analyzed using ImageJ software. The ventricular cavity was delineated in these images and both the area and major axis of the ventricular cavity were quantified.

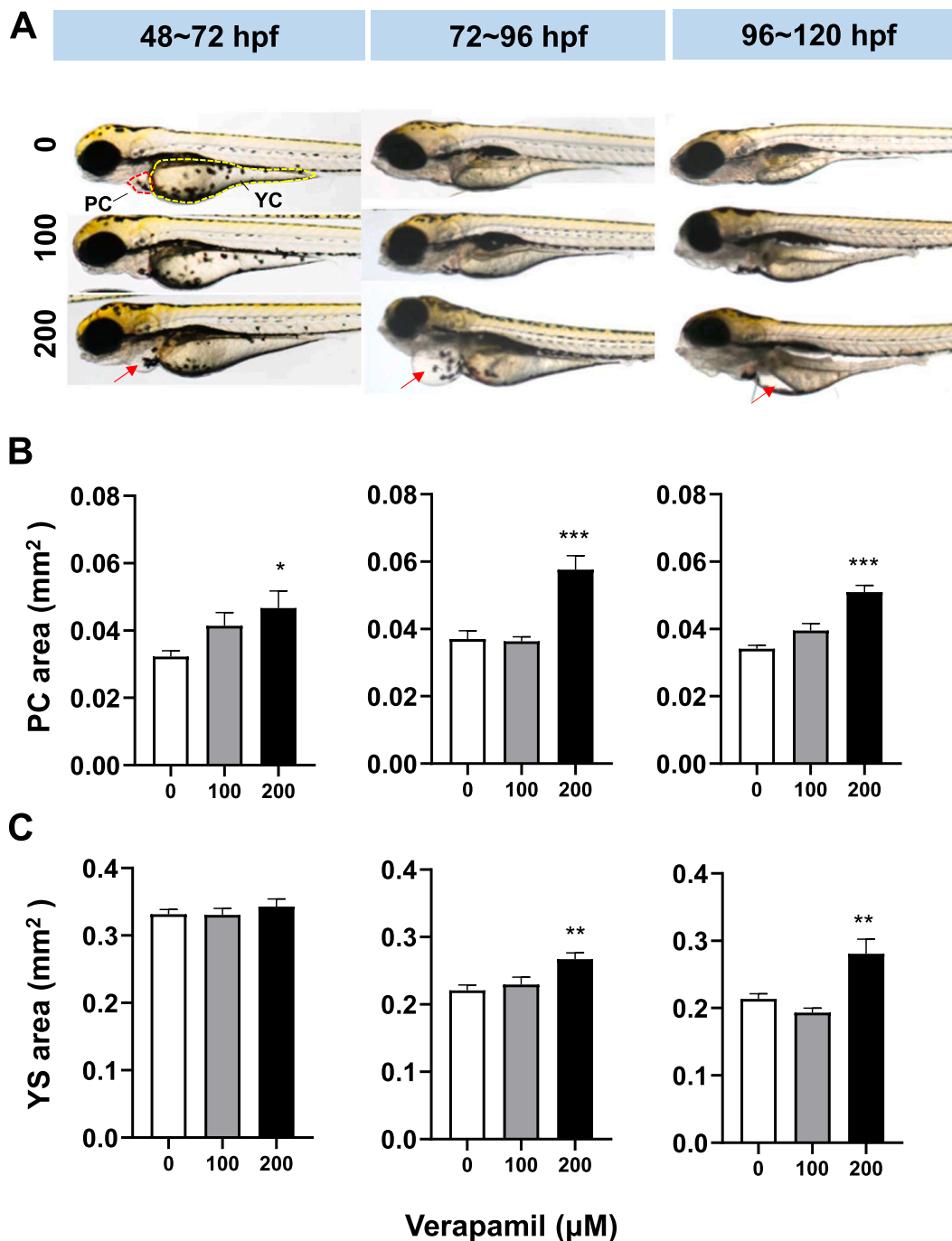


**Fig. 1.** Verapamil-induced edema in the pericardial cavity and yolk sac.

Data show three different embryonic stages (48–72, 72–96 and 96–120 h post-fertilization (hpf)) in separate columns. (A) Embryonic morphology after verapamil treatment (0, 100, and 200 μM); the pericardial cavity (PC) and yolk sac (YC) are respectively outlined in red and yellow; arrows indicate edema areas. (B) PC area and (C) YS area. Mean ± SE (n = 15 embryos). Analysis was conducted using a one-way ANOVA followed by Tukey’s pairwise comparison. \* p < 0.05; \*\* p < 0.01; \*\*\* p < 0.001.

To measure the ventricular volume, the ventricle was modeled as a prolate spheroid, and its volume was calculated from the area of an ellipse (EDA or ESA). Data from three cardiac cycles were averaged to obtain an individual value. The heart rate (HR) was determined using Tracker software by counting the number of ventricular heartbeats for 15 s. After obtaining the ED volume (EDV), ES volume (ESV), and HR, additional parameters such as stroke volume (SV), ejection fraction (EF), and cardiac output (CO) were calculated using the following formulas: SV = EDV - ESV, EF = SV / EDV, and CO = SV × HR.

### 2.5. Measurement of renal function

The renal function of zebrafish embryo was analyzed with a fluorescent clearance assay adapted from a previous study (Christou-Savina et al., 2015). Glass capillary tubes (TW 150–4; World Precision Instruments, Sarasota, FL, USA) were pulled on a flaming pipette puller (P-97; Sutter Instruments, San Rafael, CA, USA) to create micropipettes with tip diameters of 3–4 nm. These micropipettes were loaded with 50 mg/mL of 500-kDa FITC-dextran (dissolved in sterile water, Sigma-Aldrich). Using a microinjector system (IM-300, Narishigi Scientific

Instrument Laboratory, Tokyo, Japan), 1 nL of FITC-dextran was injected into the pericardial cavity of zebrafish embryos under a stereomicroscope (SZX16, Olympus, Tokyo, Japan). Dextran fluorescence of the embryos was immediately observed with an upright fluorescence

microscope (BX60, Olympus, Tokyo, Japan) equipped with a digital camera for image capture (EOS 650D, Canon, Tokyo, Japan). After 4 h of incubation in AFW, the embryos were observed and photographed again. The change in fluorescence intensity in the same embryo was measured using ImageJ software to quantify the elimination of dextran. Twelve embryos from each group ( $n = 12$ , collected from three experiments) were sampled for measurement.

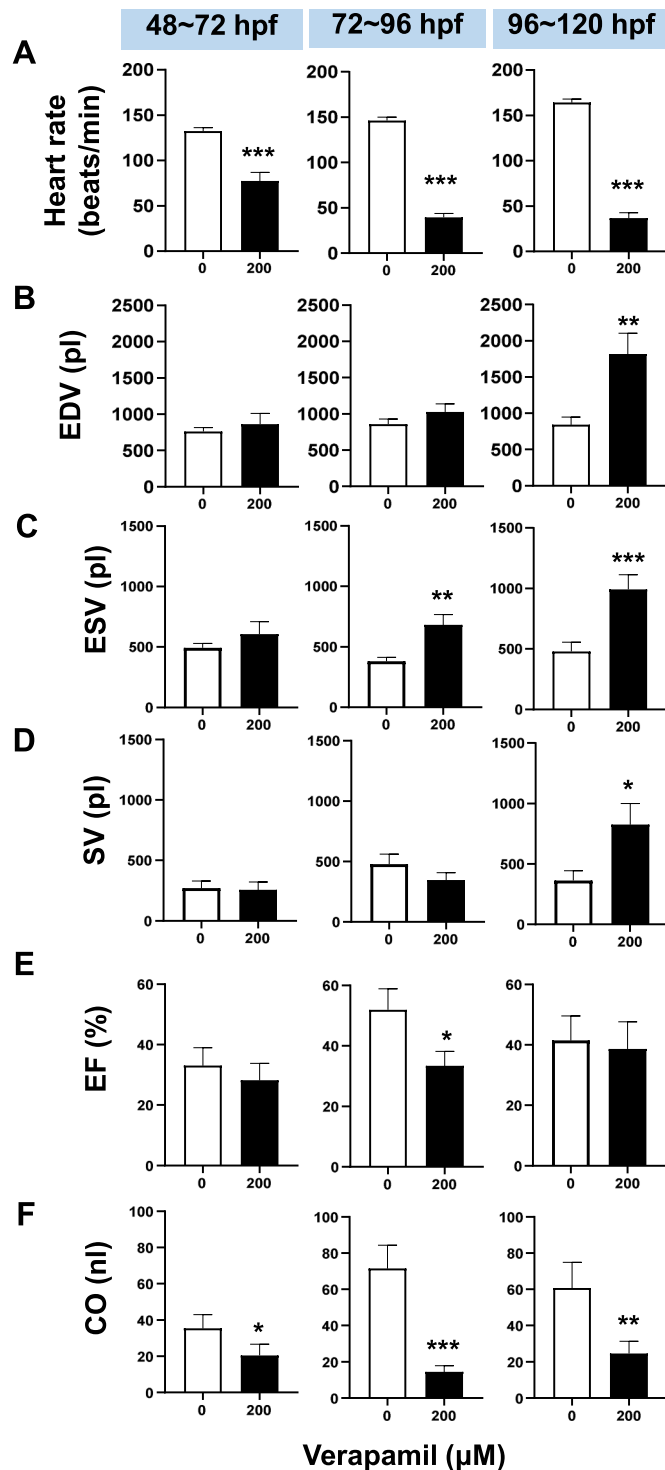


**Fig. 2.** Verapamil-induced changes in cardiac parameters. Data show three different embryonic stages (48–72, 72–96, and 96–120 h post-fertilization (hpf) in separate columns. (A) Heart rate, (B) end-diastolic volume (EDV), (C) end-systolic volume (ESV), (D) stroke volume (SV), (E) ejection fraction (EF), and (F) cardiac output (CO). Mean  $\pm$  SE ( $n = 15$  embryos). Analysis was conducted using Student's *t*-test. \*  $p < 0.05$ ; \*\*  $p < 0.01$ ; \*\*\*  $p < 0.001$ .

## 2.6. Measurement of ion contents

Sodium ( $\text{Na}^+$ ), potassium ( $\text{K}^+$ ), and calcium ( $\text{Ca}^{2+}$ ) contents in whole embryos were analyzed using inductively coupled plasma mass spectrometry (ICP-MS) following an established method (Horng et al., 2024). Each experimental group comprised a total of nine samples ( $n = 9$  from three experiments), with each sample containing ten embryos. Anesthetized embryos were rinsed with redistilled water and collected in 15-mL centrifuge tubes, to which 0.05 mL  $\text{HNO}_3$  (J.T. Baker, ThermoFisher Scientific, Waltham, MA, USA) was added. Following an incubation period at 60 °C for 12 h, digested samples were diluted with redistilled water to a final volume of 3 mL for subsequent ICP-MS analysis (Agilent 7800; Agilent Technologies, Santa Clara, CA, USA).

## 2.7. Measurement of epidermal ionocytes

Epidermal ionocyte labeling was carried out using a fluorescent mitochondrion indicator (MitoTracker), following a previously established protocol (Hung et al., 2022). A stock solution of MitoTracker Red (ThermoFisher Scientific) was diluted with AFW to a concentration of 3  $\mu\text{M}$ . Embryos were immersed in 1 mL of the MitoTracker solution for 20 min at 25 °C. Next, stained embryos were washed with AFW before being anesthetized with tricaine and examined under a fluorescent microscope (BX60, Olympus, Tokyo, Japan). The density of ionocytes in the yolk-sac area was determined by counting cell numbers within a defined square area. Fifteen embryos from each group ( $n = 15$ , collected from three experiments) were sampled for measurement.

## 2.8. Observation of ionocytes with scanning electron microscopy (SEM)

Apical openings of ionocytes in embryonic skin were observed using SEM following a previously established method (Lee et al., 2020). The SEM procedure is briefly described below. Anesthetized embryos were fixed with a solution of 4 % paraformaldehyde and 5 % glutaraldehyde at 4 °C overnight, followed by 2 % osmium tetroxide fixation at 4 °C for 2 h. Samples were then dehydrated through a series of ethanol concentrations and subjected to critical point drying. Finally, samples were examined with an SEM (Hitachi S-2400; Tokyo, Japan), and digital images were captured. The apical opening areas of ionocytes were quantified using ImageJ software. For each experimental group, 12 embryos were randomly chosen for analysis ( $n = 12$ , collected from three experiments).

## 2.9. Measurement of relative transcript levels by a real-time polymerase chain reaction (PCR)

A real-time PCR was employed to assess transcript levels of various genes, including markers for heart failure (*nppa* and *nppb*) and ion transporter genes (*rhcg1*, *slc9a3*, *atp6v1a*, *atp2b1a*, *trpv6*, and *slc12a10.2*). *rpl13a* gene was used as the reference gene for normalizing the mRNA level (Xu et al. 2016). Primer sequences for those genes are given in Supplementary Table S1. The mRNA extraction and PCR analysis procedures followed a previous study (Hsiao et al., 2024). In brief, 15 embryos were pooled to constitute one sample for mRNA extraction, utilizing the TOOLSsmart RNA extractor kit (TOOLS Biotech, New Taipei City, Taiwan). The collected mRNA samples from six such samples ( $n = 6$ ) were then converted to complementary (c)DNA using the TOOLS-Quant II Fast RT Kit (TOOLS Biotech). Following cDNA synthesis,

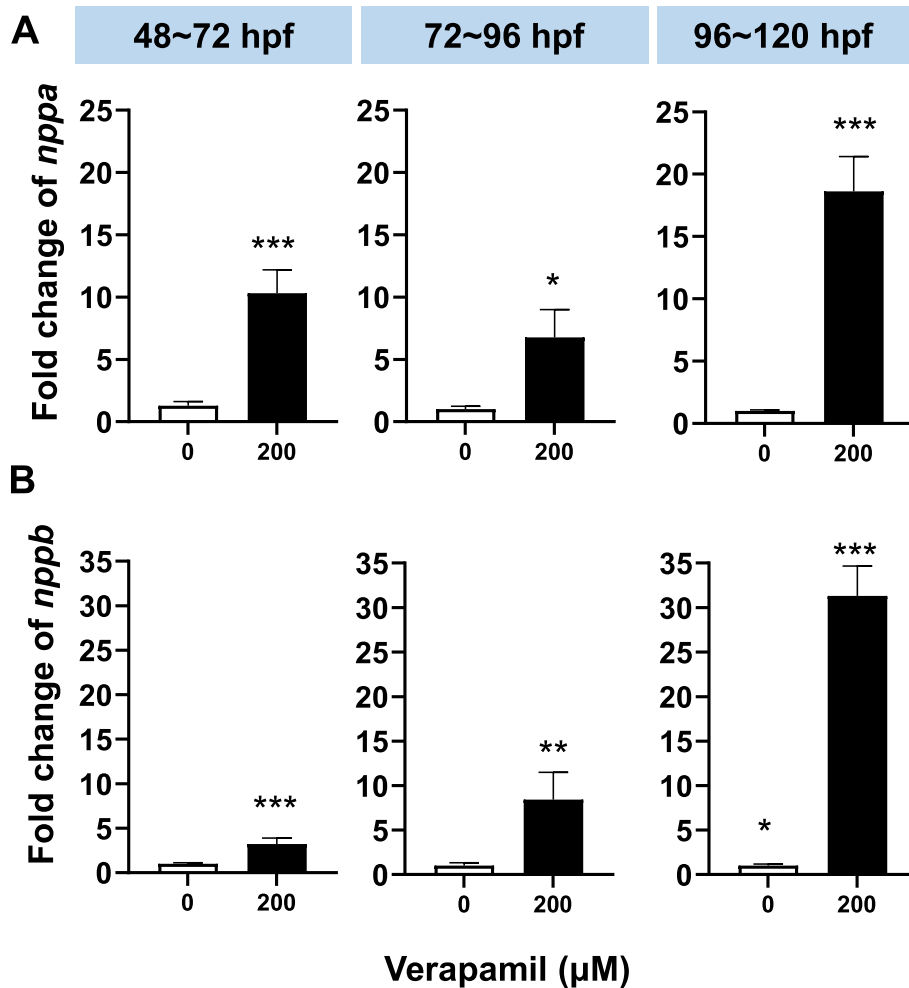


**Fig. 3.** Verapamil-induced upregulation of the *nppa* and *nppb* genes.

Data show three different embryonic stages (48–72, 72–96 and 96–120 h post-fertilization (hpf) in separate columns. (A) Fold change of *nppa* and (B) fold change of *nppb*. Mean  $\pm$  SE ( $n = 6$  samples). Analysis was conducted using Student's *t*-test. \*  $p < 0.05$ ; \*\*  $p < 0.01$ ; \*\*\*  $p < 0.001$ .

samples were appropriately diluted and analyzed using the Roche LightCycler® 480 (LC480) real-time PCR system (Roche, Basel, Switzerland).

### 2.10. Data analysis

The recorded data were plotted and statistically analyzed using GraphPad Prism software (vers. 8.0.1). Results for each group are presented in graphs showing the mean  $\pm$  standard error (SE). Before statistical analysis, the software was used to identify and exclude outliers, followed by an examination of the data distribution. The Shapiro-Wilk test was used to validate the normality of data, and Levene's test was used to check homoscedasticity. A one-way analysis of variance (ANOVA) followed by Tukey's multiple comparisons was used to compare the means of more than two groups. An independent samples *t*-test was used to compare the means between two groups.

## 3. Results

### 3.1. Evaluation of edema in embryos exposed to verapamil

Zebrafish embryos were exposed to verapamil at two concentrations (100 and 200  $\mu$ M) during three developmental stages (early: 48–72 hpf, mid: 72–96 hpf, and late: 96–120 hpf). Morphological examination revealed the initial appearance of pericardial edema followed by yolk

sac edema. Notably, later-stage embryos exhibited more-pronounced edema compared to their earlier-stage counterparts. This observation was corroborated by a morphometric analysis showing changes in the pericardial and yolk sac areas (Fig. 1A). Results showed that 100  $\mu$ M verapamil did not change the pericardial cavity area at any stage, whereas 200  $\mu$ M verapamil significantly increased the pericardial cavity area at all stages (Fig. 1B). Approximately 45 % ( $p < 0.05$ ), 57 % ( $p < 0.001$ ), and 50 % ( $p < 0.001$ ) increases were found in the early, mid, and late stages, respectively. In addition, 200  $\mu$ M verapamil did not change the yolk sac area at the early stage, but it significantly increased the yolk sac area at the mid and late stages by 25 % ( $p < 0.01$ ) and 33 % ( $p < 0.01$ ), respectively (Fig. 1C). Since 200  $\mu$ M verapamil was found to induce edema, this concentration was used in subsequent experiments.

### 3.2. Evaluation of cardiac function in embryos exposed to verapamil

After treatment with 200  $\mu$ M verapamil at three stages, the cardiac function of embryos was examined. Verapamil significantly suppressed the heart rate in all stages, with suppression in the late stage being more severe than that in the early stage (early:  $-41$  %, mid:  $-72$  %, late:  $-77$  %; all  $p < 0.001$ ; Fig. 2A). Verapamil did not change the EDV in the early or mid stages, but significantly increased the EDV by 114 % ( $p < 0.001$ ) in the late stage (Fig. 2B; images in Supplementary Fig. S1). Verapamil also increased the ESV by 79 % ( $p < 0.01$ ) and 107 % ( $p < 0.001$ ) in the mid and late stages, respectively (Fig. 2C). Because of changes in both

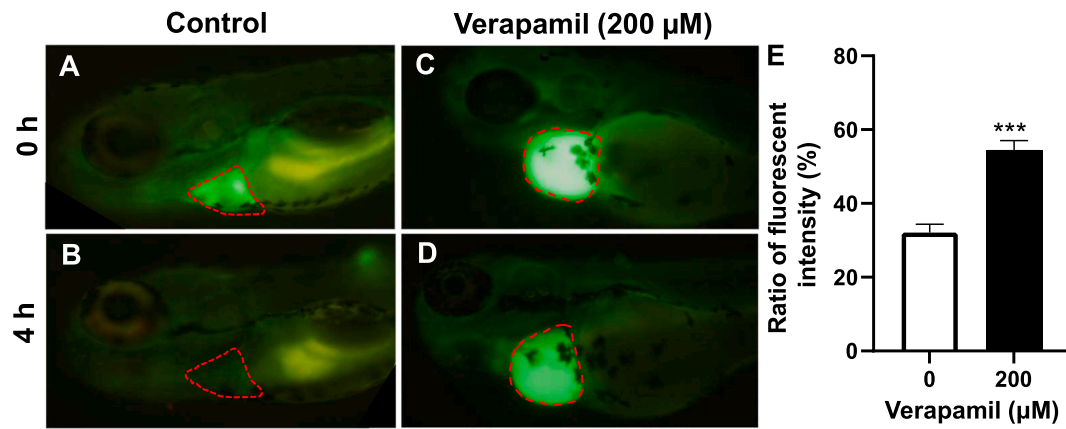


**Fig. 4.** Verapamil-induced suppression of renal FITC-dextran excretion.

Images of zebrafish embryos injected with FITC-dextran. (A) Control group at 0 h, (B) control group at 4 h, (C) verapamil group at 0 h, and (D) verapamil at 4 h. The pericardial cavity is outlined in red. The ratio of fluorescence intensity (intensity at 4 h/intensity at 0 h) of the outlined area is shown in (E). Mean  $\pm$  SE ( $n = 12$  embryos). Analysis was conducted using Student's *t*-test. \*\*\*  $p < 0.001$ .

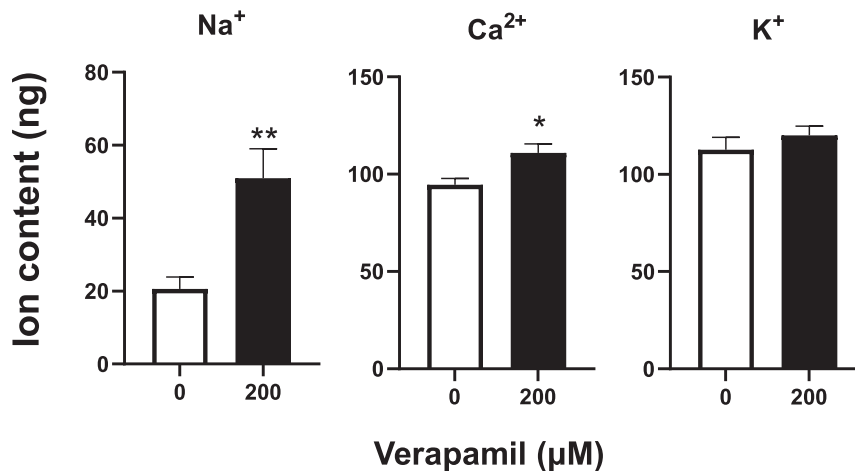


**Fig. 5.** Verapamil-induced changes in ion contents.

Ion contents (Na<sup>+</sup>, Ca<sup>2+</sup>, and K<sup>+</sup>) in whole embryos are shown. Mean  $\pm$  SE ( $n = 9$  samples). Analysis was conducted using Student's *t*-test. \*  $p < 0.05$ ; \*\*  $p < 0.01$ .

the EDV and ESV, no significant change in the SV was found at any stage (Fig. 2D), whereas a significant decrease in the EF was found in the medium stage ( $-36\%$ ;  $p < 0.05$ ; Fig. 2E). Finally, CO was significantly suppressed by 43% ( $p < 0.05$ ), 80% ( $p < 0.001$ ), and 60% ( $p < 0.01$ ) in the early, mid, and late stages, respectively (Fig. 2F).

### 3.3. mRNA levels of *nppa* and *nppb* in embryos exposed to verapamil

After treatment with 200  $\mu\text{M}$  verapamil at three stages, mRNA levels of the *nppa* and *nppb* genes of embryos were examined. Both *nppa* and *nppb* showed upregulation in all three stages. *nppa* showed fold changes of 10.3 ( $p < 0.001$ ), 6.8 ( $p < 0.05$ ), and 18.6 ( $p < 0.001$ ) in the early, mid, and late stages, while *nppb* showed fold changes of 3.2 ( $p < 0.001$ ), 8.4 ( $p < 0.01$ ), and 31.3 ( $p < 0.001$ ) in the corresponding stages (Fig. 3).

### 3.4. Renal clearance of FITC-dextran in embryos exposed to verapamil

The fluorescence signal of FITC-dextran in the pericardial cavity of embryos was assessed both before and after a 4-h elimination period (Fig. 4A, B). In the control group, the fluorescence intensity at 4 h was approximately 30% of the intensity at 0 h, indicating an elimination rate of 70% (Fig. 4C). Conversely, in the verapamil group, the ratio was approximately 55%, indicating a 45% elimination rate. Notably,

verapamil had a significant inhibitory effect ( $p < 0.001$ ) on the elimination of FITC-dextran suggesting that renal filtration was impaired.

### 3.5. Ion contents in embryos exposed to verapamil

Three major cations (sodium, calcium, and potassium) in whole embryos were examined with ICP-MS. Significant increases in sodium (2.5 fold;  $p < 0.01$ ) and calcium (1.17 fold;  $p < 0.05$ ) were found in the verapamil group (Fig. 5). The change in potassium was not significant (Fig. 5).

### 3.6. Epidermal ionocytes in embryos exposed to verapamil

Epidermal ionocytes were labeled with Mitotracker, and their density in the yolk sac region was quantified (Fig. 6A, B). No notable change was found in the morphology of ionocytes in the verapamil group, while the density of ionocytes significantly increased by 32% ( $p < 0.05$ ) in the verapamil group (Fig. 6C).

### 3.7. The apical membrane of ionocytes in embryos exposed to verapamil

SEM was employed to investigate the surface structure of epidermal ionocytes, primarily located in the yolk sac region (Fig. 7A). Exposure to

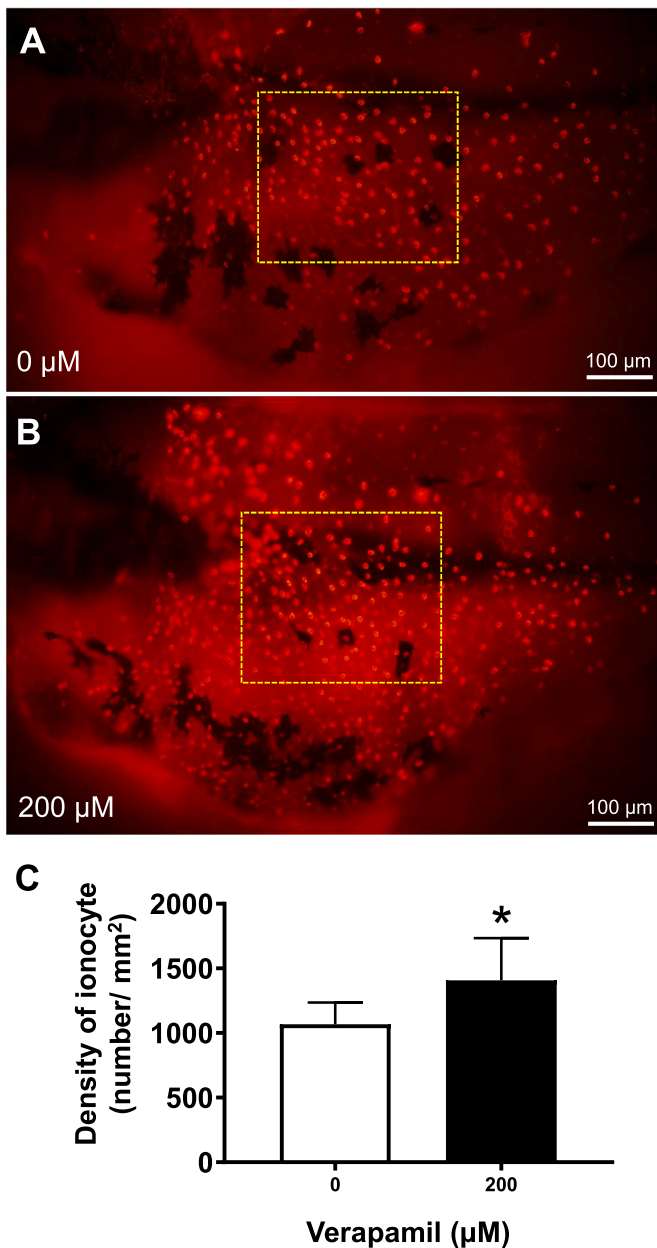


**Fig. 6.** Verapamil-induced changes in ionocyte densities. MitoTracker-labeled ionocytes in yolk sac skin are shown in (A) the control group and (B) verapamil group. A square area in the center of the yolk sac region was selected for counting the ionocyte density. (C) The density of ionocytes. Mean  $\pm$  SE ( $n = 15$  embryos). Analysis was conducted using Student's *t*-test. \*  $p < 0.05$ .

verapamil resulted in skin wrinkling due to edema in the embryos (Fig. 7B). Examination of the apical membrane of ionocytes in the yolk sac region revealed a significant increase in size in the verapamil group (2.2-fold;  $p < 0.001$ ; Fig. 7C, D).

### 3.8. mRNA levels of ion transporter genes in embryos exposed to verapamil

mRNA levels of several ion transporter genes, including *rhcg1*, *slc9a3*, *atp6v1a*, *atp2b1a*, *trpv6*, and *slc12a10.2*, were examined. All of them significantly increased in the verapamil groups with respective fold changes of 3.8 ( $p < 0.001$ ), 3.2 ( $p < 0.001$ ), 1.4 ( $p < 0.001$ ), 1.3 ( $p < 0.01$ ), 2.0 ( $p < 0.001$ ), and 2.6 ( $p < 0.001$ ) (Fig. 8).

## 4. Discussion

The exposure of zebrafish embryos to 200  $\mu$ M verapamil for 24 h resulted in edema in the pericardial cavity and yolk sac, indicating a disruption in renal water excretion. Zebrafish embryos have hypertonic body fluids (240 mOsm/L) (Charmantier et al., 2022), causing external water to perfuse and accumulate in the body cavity when renal function is compromised (Hentschel et al., 2005; Hill et al., 2004). The pericardial cavity, covered by a thin skin layer and lacking a solid tissue connection, becomes a prominent site for edema formation. As the yolk is gradually consumed during embryo development, the yolk sac may provide an additional space for water retention in later stages.

To demonstrate impaired renal function in verapamil-treated embryos, FITC-dextran (a polysaccharide) was injected into the pericardial cavity as a marker to measure the renal filtration capacity. This method was modified from the measurement of renal filtration by calculating the inulin (a polysaccharide) excretion in humans (Hentschel et al., 2005; Kotb et al., 2014). Results showed that verapamil-treated embryos had lower FITC-dextran excretion, indicating suppressed renal filtration.

Renal function, as indicated by the glomerular filtration rate, is directly proportional to the renal perfusion pressure and, therefore, to cardiac output. When cardiac output is optimal, renal perfusion is maintained at a level that supports efficient renal filtration and adequate removal of wastes and excess substances. However, when cardiac output decreases, as in conditions such as heart failure, there is a reduction in the renal perfusion pressure (Thomas et al., 1993). Indeed, the cardiac assessment in the present study showed that verapamil effectively suppressed the heart rate and thereby suppressed cardiac output. The greater suppression of cardiac output in the mid and late stages was associated with more-severe edema, particularly in the yolk sac at these stages.

Although the heart rate was suppressed by verapamil in all three stages, differential responses in the three stages were found in other cardiac parameters (EDV, ESV, and EF). A notable increase in the EDV was found in the late stage, indicating that a larger heart size (cardiomegaly) had been induced, whereas the change was not significant in the early and middle stages. The increased EDV and corresponding SV partially compensated for greater suppression of the heart rate in the late stage. In the mid-stage, however, a significant increase in the ESV was found, indicating that the contractility of the ventricular muscle was suppressed, which was reflected in a decreased EF.

The differential responses of the embryonic heart to verapamil treatment at different stages may have been due to factors such as changes in L-type calcium channel expression, maturation of the cardiac conduction system, and emergence of compensatory mechanisms. Moreover, zebrafish embryos have increased circulatory demands and renal function in later embryonic stages due to increased metabolic demands, organ development, and maturation of physiological systems (Barrionuevo and Burggren, 1999). For example, gill development gradually increases the surface area for gas exchange and it also introduces excess water into body fluids which must be efficiently excreted by the kidneys (Shadrin and Ozerniuk, 2002).

Clinically, the atrial natriuretic peptide (ANP; encoded by *nppa*) and brain natriuretic peptide (BNP; encoded by *nppb*) are biomarkers for heart failure. ANP is released by the atria in response to increased atrial pressure and regulates blood pressure and fluid balance by promoting vasodilation and excretion of sodium and water. BNP, synthesized by ventricles, is released in response to increased ventricular wall stress and serves similar functions. Elevated levels of ANP and BNP are indicative of heart failure and are used for diagnosis, assessing severity, monitoring treatment responses, and predicting outcomes (Mair et al., 2001). The elevation of *nppa* and *nppb* gene expressions in zebrafish embryos suggests that verapamil-induced heart failure may have a conserved mechanism. Moreover, the *nppa* and *nppb* genes play critical roles in the cardiac development of zebrafish (Becker et al., 2014; Grassini et al., 2018). The huge increases in expressions of these genes in the late stage

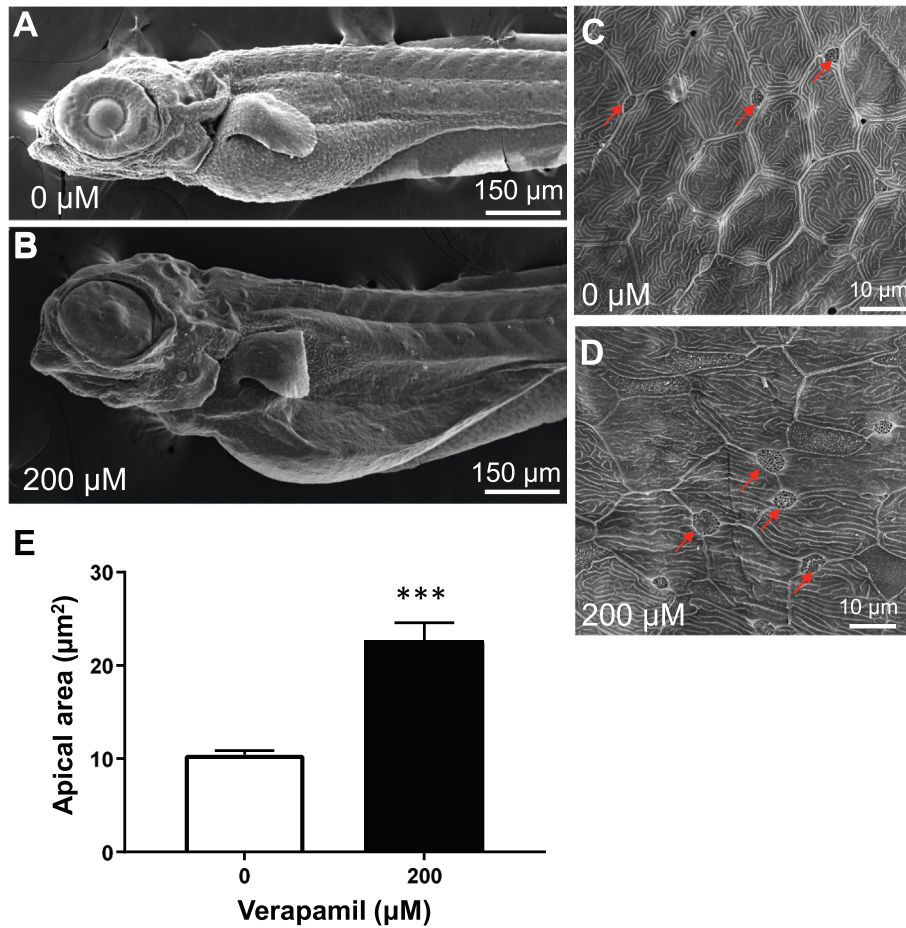


**Fig. 7.** Verapamil-induced morphological changes in ionocytes.

Scanning electronic microscopic images of embryos are shown in (A) the control group and (B) the verapamil group. The morphology of the apical membrane of ionocytes (red arrows) in the yolk sac region was examined. (C) The control group and (D) the verapamil group. (E) Quantified area of the apical membrane. Mean  $\pm$  SE ( $n = 12$  embryos). Analysis was conducted using Student's  $t$ -test. \*\*\*  $p < 0.001$ .

may be associated with the larger heart size in verapamil-treated embryos.

Verapamil-treated embryos exhibited water retention and also ion retention (particularly of sodium and calcium). This phenomenon may result from impaired renal function leading to decreased excretion of both water and ions. However, changes in levels of the three cations differed, with sodium showing a greater increase compared to calcium and potassium. This discrepancy is likely due to the naturally higher levels of sodium in plasma and interstitial fluids compared to other cations.

In addition, our observations revealed an increase in the activity of epidermal ionocytes, which are specialized cells responsible for ion uptake from water, thereby contributing to ion retention. Verapamil induced an increased density of MitoTracker-labeled ionocytes, enlargement of the ionocyte apical membrane, and upregulation of several ion transporter genes. The apical membrane refers to the membrane domain of ionocytes facing the external environment. Through ion transporters located in the apical membrane, ionocytes take up ions from water or secrete ions into water. Enlargement of the apical membrane is tightly associated with the activation of ionocytes (Horng et al., 2022; Horng et al., 2009).

The *rhcg1*, *slc9a3*, and *atp6v1a* genes respectively encode proteins known as rhesus glycoprotein, sodium-hydrogen exchanger, and V-type hydrogen pump. These proteins play essential roles in ammonia/acid excretion and sodium uptake by a specific subset of ionocytes referred to as hydrogen pump-rich cells or HR cells (Lin et al., 2006; Shih et al., 2012). Furthermore, *atp2b1a* and *trpv6* respectively encode the plasma

membrane calcium pump and epithelial calcium channel, which are vital for calcium uptake by another subtype of ionocytes known as sodium pump-rich cells or NaR cells (Lin et al., 2006; Pan et al., 2005). Additionally, *slc12a10.2* encodes the sodium-chloride cotransporter, which facilitates sodium and chloride uptake by a third subtype of ionocytes (Wang et al., 2009). Upregulation of these genes serves as molecular evidence supporting the increased sodium and calcium uptake levels by ionocytes. Elevated sodium uptake is particularly crucial for maintaining the osmolarity balance in verapamil-induced edema.

Metabolic ammonia and acid in the fish body can be eliminated by skin diffusion, ionocyte secretion, and renal excretion (Hwang and Chou, 2013; Shih et al., 2013). However, their respective proportions in fish embryos remain unknown. The significant increase in *rhcg1* and *atp6v1a* gene expressions, which encode ammonia- and acid-secreting proteins in ionocytes, suggests that verapamil-induced renal dysfunction may impair a significant portion of ammonia/acid excretion. Consequently, ionocytes are activated to compensate for this dysfunction.

Metabolic acidosis is a common symptom in patients with renal failure. The kidneys play a crucial role in maintaining the body's acid-base balance by regulating the excretion of acids ( $H^+$  and  $NH_4^+$ ) and the reabsorption of bicarbonate ( $HCO_3^-$ ). In patients with renal failure, impaired kidney function may result in insufficient removal of acids from the body, leading to metabolic acidosis (Kraut and Kurtz, 2005). The upregulation of genes such as *rhcg1* and *atp6v1a* in zebrafish embryos may represent metabolic acidosis induced by renal failure.

In this study, zebrafish embryos could tolerate verapamil exposure

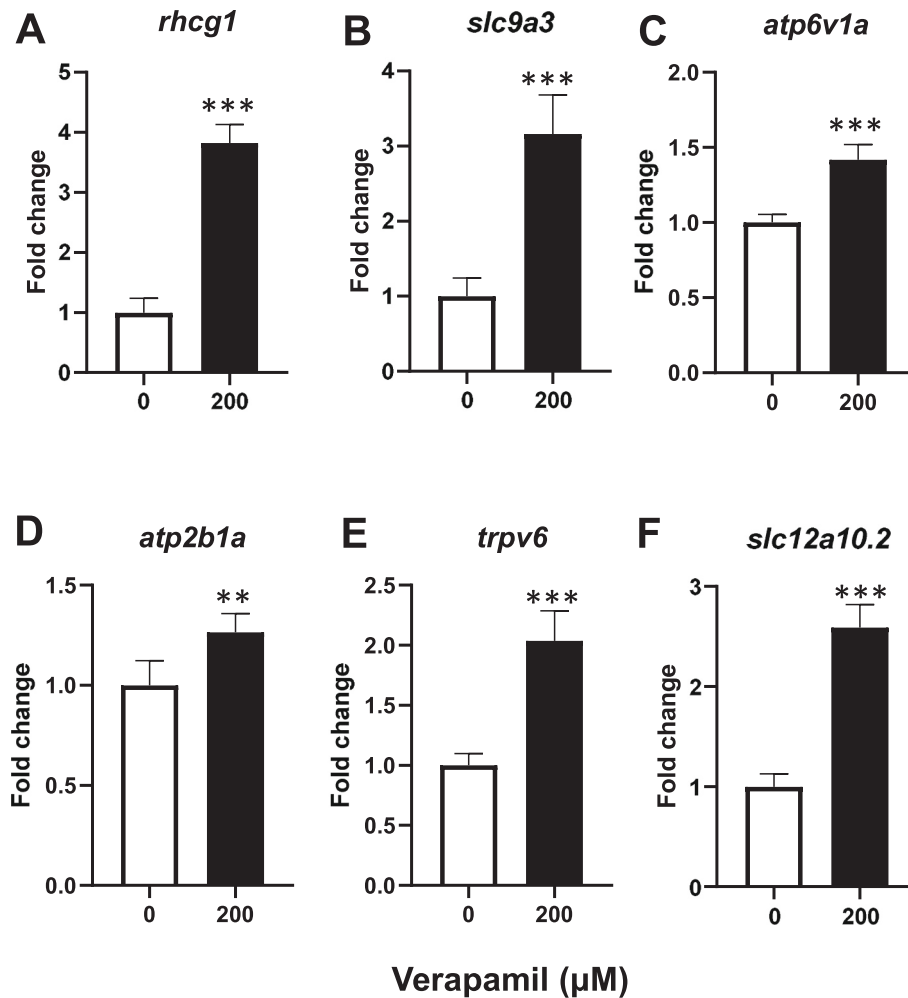


**Fig. 8.** Verapamil-induced upregulation of ion transporter genes.

Fold changes in ion transporter genes after verapamil treatment. (A) *rhcg1*, (B) *slc9a3*, (C) *atp6v1a*, (D) *atp2b1a*, (E) *trpv6*, and (F) *slc12a10.2*. Mean  $\pm$  SE ( $n = 6$  samples). Analysis was conducted using Student's *t*-test. \*  $p < 0.05$ ; \*\*  $p < 0.01$ ; \*\*\*  $p < 0.001$ .

for 24 h, a relatively long exposure time for suppressing cardiac function (–43 to –80 % CO). This is probably because oxygen diffusion alone can meet the metabolic needs of the developing embryo, even in the absence of a fully established hemoglobin-dependent oxygen transport mechanism (Pelster and Burggren, 1996). In addition, prolonged exposure to verapamil, particularly in the mid and late stages, can induce reduced contractility and cardiomegaly. Both symptoms are important clinical indicators in the diagnosis and management of heart failure. Combined with renal failure symptoms including pericardial and yolk sac edema and ion retention, this model can be used to further investigate the molecular mechanisms underlying this cardiorenal syndrome and test drugs for this disease.

The main limitation of using zebrafish to model human heart failure is the apparent lack of chronic cardiac fibrosis (Narumanchi et al., 2021). In humans, cardiac fibrosis involves the proliferation of cardiac fibroblasts, excessive extracellular matrix deposition, and macrophage activity, resulting in myocardial stiffening. This process is closely linked to cardiac remodeling after injury, such as myocardial infarction, and contributes to the development of heart failure. In contrast, zebrafish show minimal cardiac fibrosis and have cardiac regeneration capability, reducing their effectiveness for modeling chronic cardiac fibrosis.

The renin-angiotensin-aldosterone system (RAAS) plays a central role in the pathophysiology of cardiorenal syndrome (Ronco et al., 2018). In heart failure, reduced cardiac output leads to decreased renal perfusion, which triggers the release of renin from the kidneys. Renin

converts angiotensinogen to angiotensin I, which is then converted to angiotensin II. Angiotensin II causes vasoconstriction and increases aldosterone secretion, leading to increased blood pressure and fluid retention. These effects exacerbate heart failure and renal dysfunction, creating a vicious cycle of deteriorating cardiac and renal function. In the future, it is necessary to investigate the role of RAAS in this zebrafish model.

Supplementary data to this article can be found online at <https://doi.org/10.1016/j.cbpc.2024.109980>.

#### CRediT authorship contribution statement

**Jiun-Lin Horng:** Writing – review & editing, Writing – original draft, Funding acquisition, Formal analysis, Data curation, Conceptualization. **Bu-Yuan Hsiao:** Writing – review & editing, Writing – original draft, Funding acquisition, Formal analysis, Conceptualization. **Wen-Ting Lin:** Formal analysis, Data curation. **Tzu-Ting Lin:** Investigation. **Ching-Yen Chang:** Investigation. **Li-Yih Lin:** Writing – review & editing, Writing – original draft, Supervision, Project administration, Methodology, Funding acquisition, Formal analysis, Conceptualization.

#### Declaration of competing interest

The authors declare that they have no known competing financial interests or personal relationships that could have appeared to influence

the work reported in this paper.

## Data availability

Data will be made available on request.

## Acknowledgments

We express our gratitude to the National Science and Technology Council of Taiwan (NSTC 113-2321-B-003-001-) and Taipei Medical University Hospital (113TMU-TMUH-08) for their grant support.

## References

- Ali, S., Champagne, D.L., Richardson, M.K., 2012. Behavioral profiling of zebrafish embryos exposed to a panel of 60 water-soluble compounds. *Behav. Brain Res.* 228, 272–283.
- Barrionuevo, W., Burggren, W., 1999. O<sub>2</sub> consumption and heart rate in developing zebrafish (*Danio rerio*): influence of temperature and ambient O<sub>2</sub>. *Am. J. Phys.* 276, R505–R513.
- Becker, J.R., Chatterjee, S., Robinson, T.Y., Bennett, J.S., Panakova, D., Galindo, C.L., Zhong, L., Shin, J.T., Coy, S.M., Kelly, A.E., Roden, D.M., Lim, C.C., MacRae, C.A., 2014. Differential activation of natriuretic peptide receptors modulates cardiomyocyte proliferation during development. *Development* 141, 335–345.
- Charmantier, G., Nguyen-Chi, M., Lutfalla, G., 2022. Ontogenetic changes in blood osmolality during the postembryonic development of zebrafish (*Danio rerio*). *Zebrafish* 19, 1–6.
- Christou-Savina, S., Beales, P.L., Osborn, D.P., 2015. Evaluation of zebrafish kidney function using a fluorescent clearance assay. *J. Vis. Exp.* 96, e52540.
- Drummond, I.A., 2005. Kidney development and disease in the zebrafish. *J. Am. Soc. Nephrol.* 16, 299–304.
- Genge, C.E., Lin, E., Lee, L., Sheng, X., Rayani, K., Gunawan, M., Stevens, C.M., Li, A.Y., Talab, S.S., Claydon, T.W., Hove-Madsen, L., Tibbits, G.F., 2016. The zebrafish heart as a model of mammalian cardiac function. *Rev. Physiol. Biochem. Pharmacol.* 171, 99–136.
- Grassini, D.R., Lagendijk, A.K., De Angelis, J.E., Da Silva, J., Jeanes, A., Zettler, N., Bower, N.I., Hogan, B.M., Smith, K.A., 2018. Nppa and Nppb act redundantly during zebrafish cardiac development to confine AVC marker expression and reduce cardiac jelly volume. *Development* 145, dev160739.
- Groenewegen, A., Rutten, F.H., Mosterd, A., Hoes, A.W., 2020. Epidemiology of heart failure. *Eur. J. Heart Fail.* 22, 1342–1356.
- Hentschel, D.M., Park, K.M., Cilenti, L., Zervos, A.S., Drummond, I., Bonventre, J.V., 2005. Acute renal failure in zebrafish: a novel system to study a complex disease. *Am. J. Physiol. Ren. Physiol.* 288, F923–F929.
- Hill, A.J., Bello, S.M., Prasch, A.L., Peterson, R.E., Heideman, W., 2004. Water permeability and TCDD-induced edema in zebrafish early-life stages. *Toxicol. Sci.* 78, 78–87.
- Hofer, C.A., Smith, J.K., Tenholder, M.F., 1993. Verapamil intoxication: a literature review of overdoses and discussion of therapeutic options. *Am. J. Med.* 95, 431–438.
- Horng, J.L., Lin, L.Y., Hwang, P.P., 2009. Functional regulation of H<sup>+</sup>-ATPase-rich cells in zebrafish embryos acclimated to an acidic environment. *Am. J. Phys. Cell Phys.* 296, C682–C692.
- Horng, J.L., Yu, L.L., Liu, S.T., Chen, P.Y., Lin, L.Y., 2017. Potassium regulation in medaka (*Oryzias latipes*) larvae acclimated to fresh water: passive uptake and active secretion by the skin cells. *Sci. Rep.* 7, 16215.
- Horng, J.L., Lee, C.Y., Liu, S.T., Hung, G.Y., Lin, L.Y., 2022. Differential effects of silver nanoparticles on two types of mitochondrion-rich ionocytes in zebrafish embryos. *Comp. Biochem. Physiol. C Toxicol. Pharmacol.* 252, 109244.
- Horng, J.L., Kung, G.X., Lin, L.Y., 2024. Acidified water promotes silver-induced toxicity in zebrafish embryos. *Aquat. Toxicol.* 268, 106865.
- Hsiao, B.Y., Horng, J.L., Yu, C.H., Lin, W.T., Wang, Y.H., Lin, L.Y., 2024. Assessing cardiovascular toxicity in zebrafish embryos exposed to copper nanoparticles. *Comp. Biochem. Physiol. C Toxicol. Pharmacol.* 277, 109838.
- Hung, G.Y., Wu, C.L., Motoyama, C., Horng, J.L., Lin, L.Y., 2022. Zebrafish embryos as an in vivo model to investigate cisplatin-induced oxidative stress and apoptosis in mitochondrion-rich ionocytes. *Comp. Biochem. Physiol. C Toxicol. Pharmacol.* 259, 109395.
- Hwang, P.P., Chou, M.Y., 2013. Zebrafish as an animal model to study ion homeostasis. *Pflugers Arch.* 465, 1233–1247.
- Hwang, P.P., Lin, L.Y., 2013. Gill ionic transport, acid-base regulation, and nitrogen excretion. *Physiol. Fish.* 4, 205–233.
- Hwang, P.P., Lee, T.H., Lin, L.Y., 2011. Ion regulation in fish gills: recent progress in the cellular and molecular mechanisms. *Am. J. Phys. Regul. Integr. Comp. Phys.* 301, R28–R47.
- Kemp, C.D., Conte, J.V., 2012. The pathophysiology of heart failure. *Cardiovasc. Pathol.* 21, 365–371.
- Kithcart, A., MacRae, C.A., 2017. Using zebrafish for high-throughput screening of novel cardiovascular drugs. *JACC Basic Transl. Sci.* 2, 1–12.
- Kotb, A.M., Muller, T., Xie, J., Anand-Apte, B., Endlich, K., Endlich, N., 2014. Simultaneous assessment of glomerular filtration and barrier function in live zebrafish. *Am. J. Physiol. Ren. Physiol.* 307, F1427–F1434.
- Kraut, J.A., Kurtz, I., 2005. Metabolic acidosis of CKD: diagnosis, clinical characteristics, and treatment. *Am. J. Kidney Dis.* 45, 978–993.
- Lee, C.Y., Horng, J.L., Liu, S.T., Lin, L.Y., 2020. Exposure to copper nanoparticles impairs ion uptake, and acid and ammonia excretion by ionocytes in zebrafish embryos. *Chemosphere* 261, 128051.
- Li, J., Zhu, Y., Zhao, X., Zhao, L., Wang, Y., Yang, Z., 2022. Screening of anti-heart failure active compounds from fangjihuangqi decoction in verapamil-induced zebrafish model by anti-heart failure index approach. *Front. Pharmacol.* 13, 999950.
- Lin, L.Y., Horng, J.L., Kunkel, J.G., Hwang, P.P., 2006. Proton pump-rich cell secretes acid in skin of zebrafish larvae. *Am. J. Phys. Cell Phys.* 290, C371–C378.
- Lin, L.-Y., Hung, G.-Y., Yeh, Y.-H., Chen, S.-W., Horng, J.-L., 2019. Acidified water impairs the lateral line system of zebrafish embryos. *Aquat. Toxicol.* 217, 105351.
- Mair, J., Hammerer-Lercher, A., Puschedorf, B., 2001. The impact of cardiac natriuretic peptide determination on the diagnosis and management of heart failure. *Clin. Chem. Lab. Med.* 39, 571–588.
- Narumanchi, S., Wang, H., Perttunen, S., Tikkanen, I., Lakkisto, P., Paavola, J., 2021. Zebrafish heart failure models. *Front. Cell Dev. Biol.* 9, 662583.
- Pan, T.C., Liao, B.K., Huang, C.J., Lin, L.Y., Hwang, P.P., 2005. Epithelial Ca<sup>2+</sup> channel expression and Ca<sup>2+</sup> uptake in developing zebrafish. *Am. J. Phys. Regul. Integr. Comp. Phys.* 289, R1202–R1211.
- Pelster, B., Burggren, W.W., 1996. Disruption of hemoglobin oxygen transport does not impact oxygen-dependent physiological processes in developing embryos of zebrafish (*Danio rerio*). *Circ. Res.* 79, 358–362.
- Poureetezadi, S.J., Wingert, R.A., 2016. Little fish, big catch: zebrafish as a model for kidney disease. *Kidney Int.* 89, 1204–1210.
- Ronco, C., Bellasi, A., Di Lullo, L., 2018. Cardiorenal syndrome: an overview. *Adv. Chronic Kidney Dis.* 25, 382–390.
- Shadrin, A.M., Ozerniuk, N.D., 2002. Development of the gill system in early ontogenesis of Danio and nine spike stickleback. *Ontogeny* 33, 118–123.
- Shih, T.H., Horng, J.L., Liu, S.T., Hwang, P.P., Lin, L.Y., 2012. Rhcg1 and NHE3b are involved in ammonium-dependent sodium uptake by zebrafish larvae acclimated to low-sodium water. *Am. J. Phys. Regul. Integr. Comp. Phys.* 302, R84–R93.
- Shih, T.H., Horng, J.L., Lai, Y.T., Lin, L.Y., 2013. Rhcg1 and Rhbg mediate ammonia excretion by ionocytes and keratinocytes in the skin of zebrafish larvae: H<sup>+</sup>-ATPase-linked active ammonia excretion by ionocytes. *Am. J. Phys. Regul. Integr. Comp. Phys.* 304, R1130–R1138.
- Strähle, U., Scholz, S., Geisler, R., Greiner, P., Hollert, H., Rastegar, S., Schumacher, A., Selderslaghs, I., Weiss, C., Witters, H., 2012. Zebrafish embryos as an alternative to animal experiments—a commentary on the definition of the onset of protected life stages in animal welfare regulations. *Reprod. Toxicol.* 33, 128–132.
- Thomas, S.G., Paterson, D.H., Cunningham, D.A., McLellan, D.G., Kostuk, W.J., 1993. Cardiac output and left ventricular function in response to exercise in older men. *Can. J. Physiol. Pharmacol.* 71, 136–144.
- Wang, Y.F., Tseng, Y.C., Yan, J.J., Hiroi, J., Hwang, P.P., 2009. Role of SLC12A10.2, a Na-Cl cotransporter-like protein, in a Cl uptake mechanism in zebrafish (*Danio rerio*). *Am. J. Phys. Regul. Integr. Comp. Phys.* 296, R1650–R1660.
- Yalcin, H.C., Amindari, A., Butcher, J.T., Althani, A., Yacoub, M., 2017. Heart function and hemodynamic analysis for zebrafish embryos. *Dev. Dyn.* 246, 868–880.
- Zhu, X.Y., Wu, S.Q., Guo, S.Y., Yang, H., Xia, B., Li, P., Li, C.Q., 2018. A zebrafish heart failure model for assessing therapeutic agents. *Zebrafish* 15, 243–253.
- Zon, L.I., Peterson, R.T., 2005. In vivo drug discovery in the zebrafish. *Nat. Rev. Drug Discov.* 4, 35–44.